

# Particle Methods

Autor: Prof. Dr. habil. Heinz Konietzky, Dr. Christin Jakob  
(TU Bergakademie Freiberg, Geotechnical Institute)

---

1	Introduction.....	2
2	Discrete Elements .....	3
2.1	Contact detection.....	3
2.2	Contact laws.....	4
2.3	Physics of DEM-Particles .....	5
2.4	Time integration.....	8
2.5	More complex approaches .....	8
2.6	Examples.....	10
3	Smoothed Particles .....	14
3.1	Interpolation.....	14
3.2	Physics of SPH-Particles.....	15
3.3	Examples.....	16
4	Lattice Boltzmann.....	17
4.1	Boltzmann equation.....	17
4.2	Time relaxation according to Bhatnagar, Gross and Krook .....	18
4.3	Examples.....	19
5	Molecular Dynamics .....	21
5.1	Schrödinger equation .....	21
5.2	Potentials.....	21
5.3	Physics of MD-Particles.....	23
5.4	Examples.....	23
	References .....	24

# 1 Introduction

## ***What are particle methods?***

Numerical calculation methods can be divided into:

- Explicit and implicit methods in terms of time discretization
- Continuum mechanical (meshbased) and discontinuum mechanical (meshfree) methods in terms of spatial discretization

All methods can be executed independent of spatial discretization as implicit or explicit calculations. Typical representatives of meshbased methods are FEM (Finite Element Method), REM (Rand Element Method) or VEM (Volume Element Method). Typical representatives of meshfree methods are DEM (Discrete Element Method), SPH (Smooth Particle Hydrodynamics) or MD (Molecular Dynamics).

While in classical continuum mechanics coherence of the body (continuum) is maintained (neighbor relations maintain resp. will be predefined), discontinuum mechanics allows the inspection of interactions of several single bodies (continua). Therefore these methods require an automated contact detection algorithm as well as corresponding contact laws, that get active during interaction (physical or as field force over far distances).

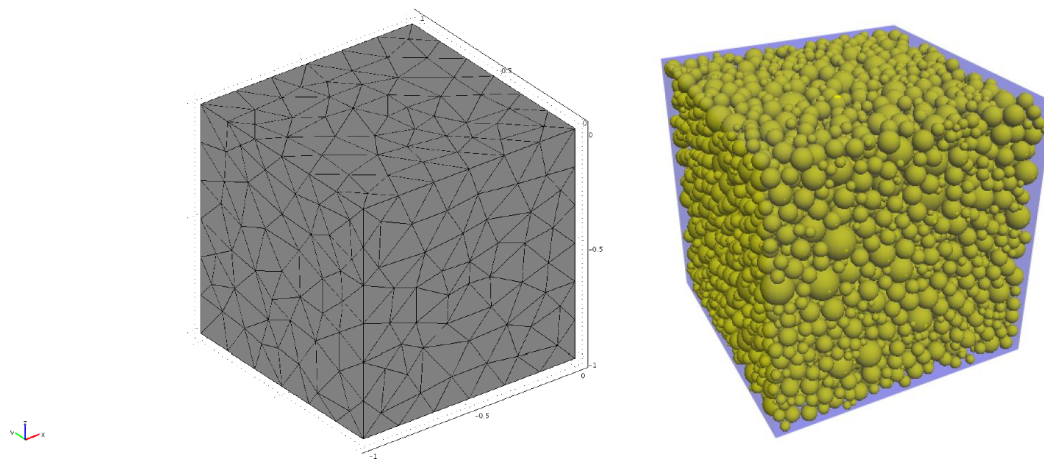


Fig. 1.1: Model examples for finite (left) and discrete elements (right), (source: Chair for rock mechanics, TU Bergakademie Freiberg)

## ***Where are particle methods used?***

- Simulation of granular media and hard rocks (DEM)
- Fluid simulations (SPH, LBM)
- Simulation of molecules and nanoparticles (MD)
- Calculations for astrophysics (SPH)

## 2 Discrete Elements

Discrete Element Method (DEM) is a particle method based on Newton's laws of motion. Particles can move with six degrees of freedom (three for translational and three for rotational movement). Particles are rigid and hence not deformable. In principle particles can have every arbitrarily geometrical shape, in which sphere shape is most efficient from numerical point of view. When particles come in contact forces (depending on the chosen contact law) start acting on them. Furthermore external forces (e.g. gravity) can act on the particles. During a calculation contacts can be formed or break. Thus an efficient automated contact detection is one of the core components of a DEM-Software. Modelling with discrete elements take place in six phases:

1. Generation of particles + definition of boundary and initial conditions
2. Determination of contacts (between particles and between particles and boundary)
3. Calculation of forces  $F$  and moments  $M$  of all particles
4. Calculation of accelerations  $\ddot{u}$  and  $\dot{\omega}$ , velocities  $\dot{u}$  and  $\omega$ , and displacements  $u$  and rotations of all particles
5. Calculation of new positions  $x$  of all particles
6. Repeat step 2. to 5. with time step  $\Delta t$  until stop criterion is achieved

Pioneer work to development of discrete resp. distinct elements was mainly provided by Peter A. Cundall, who improved and extended this method in numerous publications. Since 1995 DEM-Software PFC (Particle Flow Code) from company Itasca is available. With this code two-dimensional (PFC2D) as well as three-dimensional (PFC3D) models can be calculated. Following description mainly depends on manuals from this software.

### 2.1 Contact detection

Computing time for contact detection increases quadratically with the amount of particles in the model. Therefore it is necessary to use an optimized contact detection algorithm for DEM. Thereby all non-possible contacts will be sorted out in the first step. In the second step a more detailed procedure (computationally more intensive) analyzes, if remaining possible contacts are real contacts. When a real contact is found, contact law is applied to calculate the contact forces (see section 2.2).

Pre-sort processes can be divided in cellbased methods and methods with Verlet lists (Fig. 2.1). In cellbased methods the model is splitted into smaller axis-aligned cells. The bigger the cells, the more possible contacts are pre-sorted. That leads to higher computing time. The smaller the cells, the more cells must be scanned, whereby also more computing time is needed. In the most DEM-Codes an optimal cell size is estimated by a heuristic method when the model is initialized. Applying method with Verlet lists a monitoring radius, including all possible contact neighbors, is assigned to every particle.

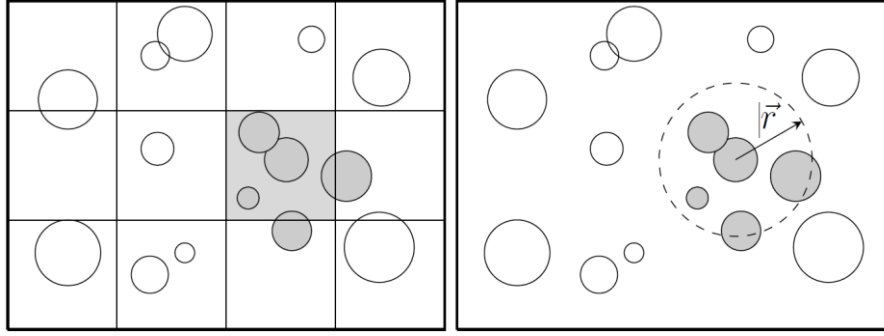





Fig. 2.1: Cellbased method (left) and method with Verlet lists (right)

## 2.2 Contact laws

When two particles come in contact, acting forces were calculated by a contact law. Contact laws are built by different basic elements, that can be visualized with a circuit diagram. The basic elements are the spring , the viscous dashpot  and the frictional slider  (also called frictional resistance or shear slider). In a pure elastic law contact force is described by two springs (see 2.2) with stiffnesses  $k_n$  for normal direction and  $k_s$  for shear direction.

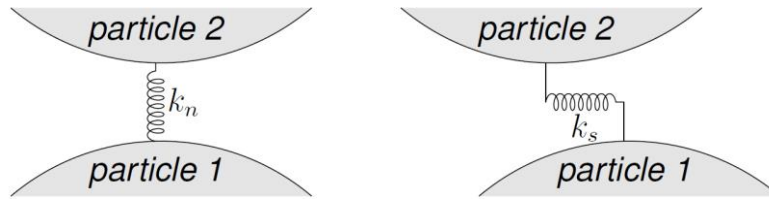


Fig. 2.2: Elastic contact law

The normal contact force  $F_n$  in the linear-elastic contact law is the product of constant normal stiffness  $k_n$  and overlap  $u_n$ .

$$F_n = k_n u_n \quad (1)$$

The updated shear contact force  $F_s^{\text{new}}$  arises from the sum of the shear contact force of the previous time step  $F_s^{\text{old}}$  and the update value  $\Delta F_s$ .

$$F_s^{\text{new}} = F_s^{\text{old}} + \Delta F_s \quad \text{with} \quad \Delta F_s = -k_s \cdot \Delta u_s \quad (2)$$

At non-linear Hertz-Mindlin contact law stiffnesses  $k_n$  and  $k_s$  are calculated according to input parameter shear modulus  $G$ , Poisson ratio  $\nu$ , the radii of particles  $R_1$  and  $R_2$  and the amount of overlap  $u_n$ .

$$k_n = \left( \frac{G\sqrt{2R_d}}{(1-\nu)} \right) \sqrt{u_n} \quad \text{with} \quad R_d = \frac{2R_1R_2}{R_1 + R_2} \quad (3)$$

$$k_s = \left( \frac{2(3G^2(1-\nu)R_d)^{\frac{1}{3}}}{2-\nu} \right) \cdot (F_n)^{\frac{1}{3}} \quad (4)$$

Every mechanical system “looses” energy (e.g. in terms of thermal energy with friction or plastic deformation). For taking account of this loss of energy during particle contact in the model, a damping element is connected in parallel to the spring in the contact law. In the case of shearing energy disappears because of frictional sliding. Hence a frictional slider is connected in series in the contact law (see 2.3).

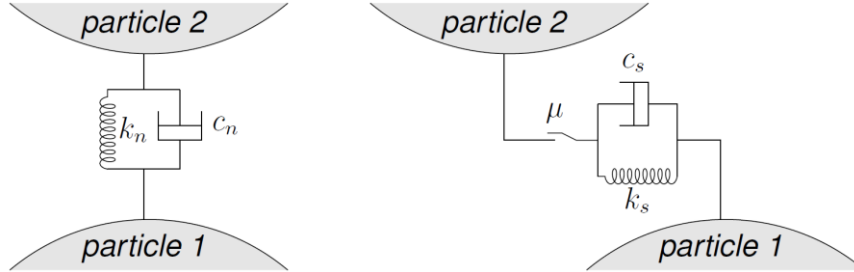


Fig. 2.3: Contact law with viscous damping and frictional slider

Damping acts proportional to velocity at normal contact force  $F_n$ , hence the amount of viscous damping  $c_n \dot{u}_n$  must be added to  $F_n$ .

$$F_n = k_n u_n - c_n \dot{u}_n \quad (5)$$

Also the update of shear contact force  $\Delta F_s$  must be added by the amount of viscous damping for shear direction  $c_s \Delta \dot{u}_s$ .

$$\Delta F_s = -k_s \cdot \Delta u_s - c_s \cdot \Delta \dot{u}_s \quad (6)$$

Here  $c_n$  and  $c_s$  are the normal and shear damping coefficients.  $c_n$  (resp.  $c_s$ ) is the product of damping ratio  $\beta_n$  (resp.  $\beta_s$ ) and critical damping constant  $c_n^{\text{crit}}$  (resp.  $c_s^{\text{crit}}$ ).  $c_n$  is given by

$$c_n = \beta_n c_n^{\text{crit}} = 2\beta_n \sqrt{mk_n} \quad (7)$$

where  $m$  is the effective mass of the system. The calculation for  $c_s$  happens analog. The sliding behavior during shear movement is described by friction coefficient  $\mu$ .  $\mu$  is defined as ratio of maximum shear contact force  $F_s^{\text{max}}$  to normal contact force and limits shear contact force in case of sliding to

$$F_s^{\text{max}} = \mu |F_n| \quad (8)$$

### 2.3 Physics of DEM-Particles

In the following the description of physics of two DEM particles in contact is given. The used notations are shown in Fig. 2.4.

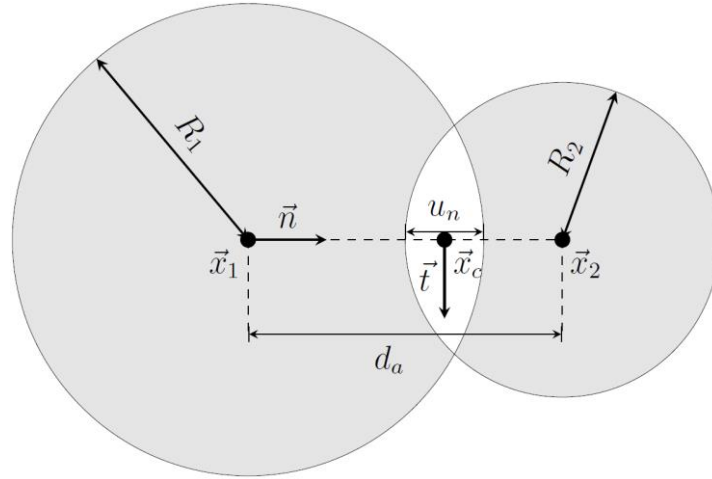


Fig. 2.4: Contact of two particles in a DEM model

Vectors  $\vec{x}_1$  and  $\vec{x}_2$  are position vectors from particle centres and  $\vec{n}$  and  $\vec{t}$  denote the normal resp. tangential unity vectors. The following relations arise (see Fig. 2.4).

$$d_a = |\vec{x}_2 - \vec{x}_1| \quad \vec{n} = \frac{\vec{x}_2 - \vec{x}_1}{d_a} \quad u_n = R_1 + R_2 - d_a \quad (9)$$

The position vector of contact point  $\vec{x}_c$  results as follows.

$$\vec{x}_c = \vec{x}_1 + (R_1 - 1/2 \cdot u_n) \cdot \vec{n} \quad (10)$$

With stiffnesses  $k_n$  and  $k_s$  the normal and shear component of contact force  $F_c$  are determined. The normal component is calculated directly during creation of the contact.

The shear component at this time is zero. It is increased (resp. decreased) by  $\Delta F_s$  at each time step.

$$\Delta F_s = -k_s \cdot \Delta u_s \quad \text{and} \quad F_n = k_n u_n \quad (11)$$

The amount of shear displacement at each time step  $\Delta u_s$  is described at the end of this section in Eq. (21). The contact force between two particles is then determined by

$$\vec{F}_c = F_n \cdot \vec{n} + F_s \cdot \vec{t} \quad (12)$$

Total force  $\vec{F}$  ( $\square F_i$ ), that acts on one particle, is composed of the sum of all contact forces from neighbor particles and gravity force  $\vec{F}_g = m \cdot \vec{g}$ .

$$\vec{F} = \sum_c \vec{F}_c + \vec{F}_g \quad (13)$$

Total force in  $i$ -direction ( $i \in \{1, 2, 3\}$ )  $F_i$ , that acts on one particle, is determined by Newton's second law (fundamental law of dynamics).  $F_i$  is calculated by multiplication of the particle mass  $m$  and the sum of its accelerations ( $\ddot{u}_i$  and  $g_i$ ).

$$F_i = m \cdot (\ddot{u}_i + g_i) \quad (14)$$

Eq. (15) arises from rearranging Eq. (14).

$$\ddot{u}_i = \frac{F_i}{m} - g_i \quad (15)$$

After double integration with respect to time  $t$  velocity  $\dot{u}_i$  and displacement  $u_i$  are determined.

$$\dot{u}_i = \int \ddot{u}_i dt \quad \text{and} \quad u_i = \int \dot{u}_i dt \quad (16)$$

For description of rotational movement vector  $\vec{r}_c$  is introduced.  $\vec{r}_c$  connects the particle centre with the contact point. Therefore torsional moment  $\vec{M}$  arises from following relation.

$$\vec{M} = \sum_c (\vec{r}_c \times \vec{F}_c) \quad \text{with} \quad \vec{r}_c = \vec{x}_c - \vec{x} \quad \text{and} \quad \vec{x} = \vec{x}_1 \quad (\text{for particle 1}) \quad (17)$$

Torsional moment in  $i$ -direction  $M_i$  is determined by multiplication of moment of inertia  $J$  and angular acceleration  $\dot{\omega}_i$ .

$$M_i = J \cdot \dot{\omega}_i \quad (18)$$

Moment of inertia is given by  $J = 2/5 mR^2$ , because all particles are spheres. By rearranging and integration with respect to  $t$  one gets angular acceleration  $\omega_i$ .

$$\omega_i = \int \frac{5M_i}{2mR^2} dt \quad (19)$$

With velocities  $\vec{v}_1 \square \dot{u}_{i1}$  and  $\vec{v}_2 \square \dot{u}_{i2}$  and angular accelerations  $\vec{\omega}_1$  and  $\vec{\omega}_2$  relative velocity  $\vec{v}_{\text{rel}}$  is computed.

$$\vec{v}_{\text{rel}} = (\vec{v}_2 + \vec{\omega}_2 \times (\vec{x}_c - \vec{x}_2)) - (\vec{v}_1 + \vec{\omega}_1 \times (\vec{x}_c - \vec{x}_1)) \quad (20)$$

Shear displacement at each time step  $\Delta u_s$  from Eq. (11) is calculated by multiplication of shear velocity  $v_s$  with time step  $\Delta t$ .  $v_s$  is calculated by relative velocity  $v_{\text{rel}} = |\vec{v}_{\text{rel}}|$  by subtracting normal velocity.

$$\Delta u_s = v_s \Delta t \quad \text{with} \quad v_s = v_{\text{rel}} - v_n \quad \text{and} \quad v_n = |\vec{v}_{\text{rel}} \cdot \vec{n}| \quad (21)$$

## 2.4 Time integration

PFC calculates velocities  $\dot{x}_i$  and  $\omega_i$  at averaged time intervals  $t \pm \Delta t/2$  and values for  $x_i$ ,  $\ddot{x}_i$ ,  $\dot{\omega}_i$ ,  $F_i$  and  $M_i$  at primary intervals  $t \pm \Delta t$ . Numerical solution of integrations from Eq. (16) and (19) is done with central difference quotient

$$\ddot{u}_i^{(t)} = \frac{1}{\Delta t} \left( \dot{u}_i^{(t+\Delta t/2)} - \dot{u}_i^{(t-\Delta t/2)} \right) \quad \text{and} \quad \dot{\omega}_i^{(t)} = \frac{1}{\Delta t} \left( \omega_i^{(t+\Delta t/2)} - \omega_i^{(t-\Delta t/2)} \right) \quad (22)$$

From the Eq. (22), (15) and (18) the “new” velocities at time  $t + \Delta t/2$

$$\dot{u}_i^{(t+\Delta t/2)} = \dot{u}_i^{(t-\Delta t/2)} + \left( \frac{F_i^{(t)}}{m} + g_i \right) \Delta t \quad \text{and} \quad \omega_i^{(t+\Delta t/2)} = \omega_i^{(t-\Delta t/2)} + \left( \frac{5M_i^{(t)}}{2mR^2} \right) \Delta t \quad (23)$$

and the “new” particle positions at time  $t + \Delta t$  are determined.

$$x_i^{(t+\Delta t)} = x_i^{(t)} + \dot{u}_i^{(t+\Delta t/2)} \Delta t \quad (24)$$

Again beginning at Eq. (9) forces and displacements for next time step are computed with these new positions. For complete numerical description of motion and contact behavior see to PFC manual (Itasca 2008).

## 2.5 More complex approaches

The particle approaches based on rigid spheres can be extended in many respects:

**Clumps** can be formed out of two or more particles. With it more complex particle shapes can be created.

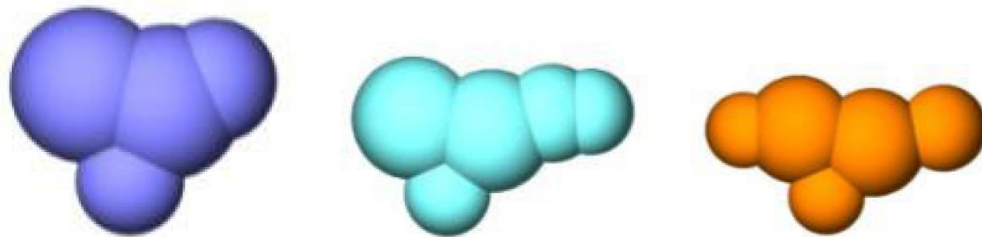


Fig. 2.5: Examples for clumps created by overlapping spheres (source: Chair for rock mechanics, TU Bergakademie Freiberg)

**Bonds** are linkages with that particles can be cohesively connected. In doing so several particles can be bonded to a grain (or cluster), that can break along cohesive bonds at according action. Hence it is possible to simulate solids like ceramics, concrete or hard rocks and also solid bridges between granular media.



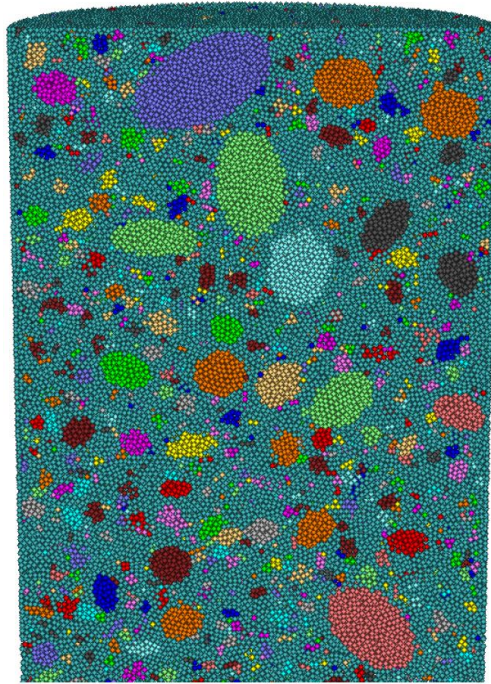


Fig. 2.6: Solid body consisting of spherical particles and different-sized particles, that are built up of several spheres (Cluster) (source: Chair for rock mechanics, TU Bergakademie Freiberg)

**Model boundaries** are defined by planes and/or by particles itself. Planes can be rectangles, but they can also have more complex geometries (consisting of triangular partial planes). Particles can be used as boundary by fixing them (limitation of degrees of freedom) or by defining periodic boundaries. In the case of periodic boundaries particles, that touch the boundary box, are getting master particles. Every of these master particles generates one slave particle on the opposite side of the boundary. Thus the model is leaning on itself at the boundary.

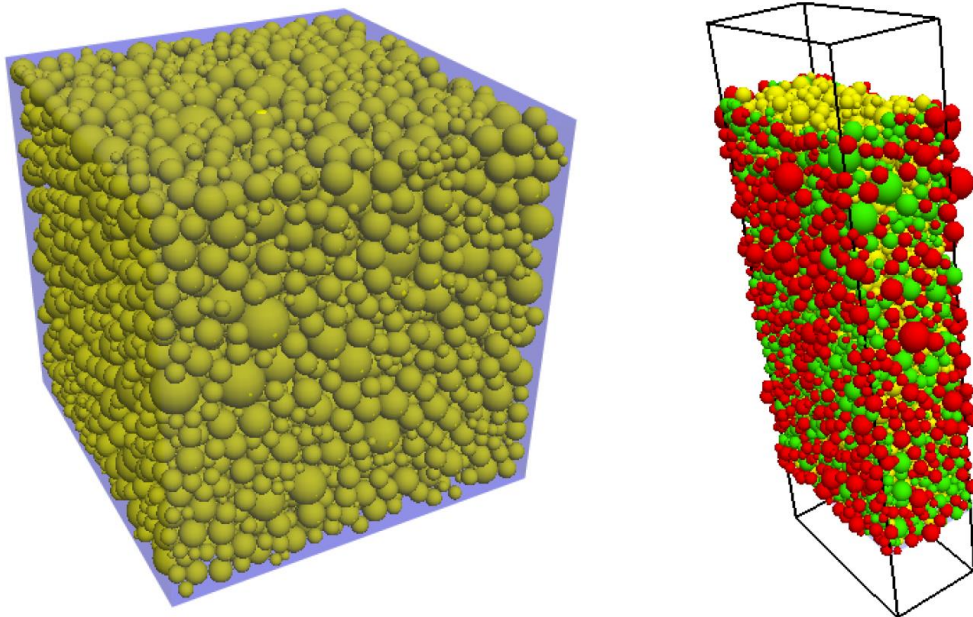
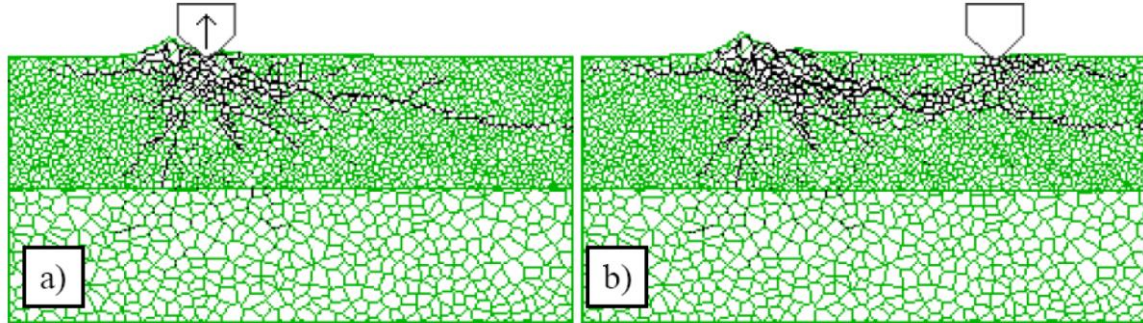


Fig. 2.7: DEM model with different boundaries, planes (left) and periodic boundary (right)

## 2.6 Examples

DEM permits to observe a solid body with respect of its deformation, stress and resistance behavior including crack propagation (see 2.8).



Fracture propagation with a blunt bit a) after the first penetration at a depth at 1.27 mm, b) at a cutting distance of 76 mm and a depth of 0.9 mm

Fig. 2.8: Intrusion of a wedge into a solid body consisting of Voronoi-particles, with crack propagation (source: Chair for rock mechanics, TU Bergakademie Freiberg)

By using bonds cementations between sand grains, like they are present in sandstone, can be simulated. Following example shows a sample (left) and its broken bonds, that result from a shear fracture (visualized by grey cylinders).

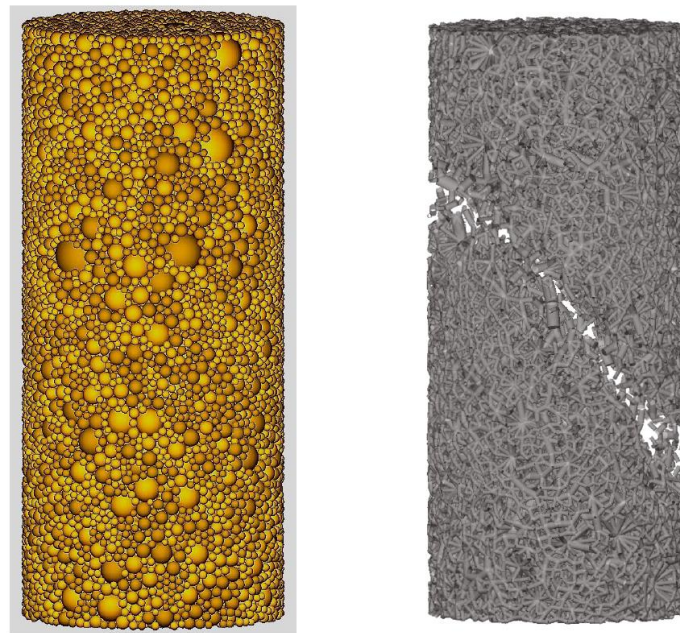


Fig. 2.9: Sandstone sample, setting (left) and cohesive bonds after shear fracture (right), (source: Chair for rock mechanics, TU Bergakademie Freiberg)

Zhang & Konietzky (2025) used DEM to investigate the force chain evolution of granular solids (rock-like material) at the grain size level during compressive loading. These simulations illustrate how the internal microstructure influence the stress distribution and damage evolution. It also becomes visible how increasing loading level influence the internal stress redistributions governed by damage evolution. They also document the increasing anisotropy and inhomogeneity with increasing stress level and the reorientation of contact stresses at the grain size level. See Fig. 2.10-2.15.



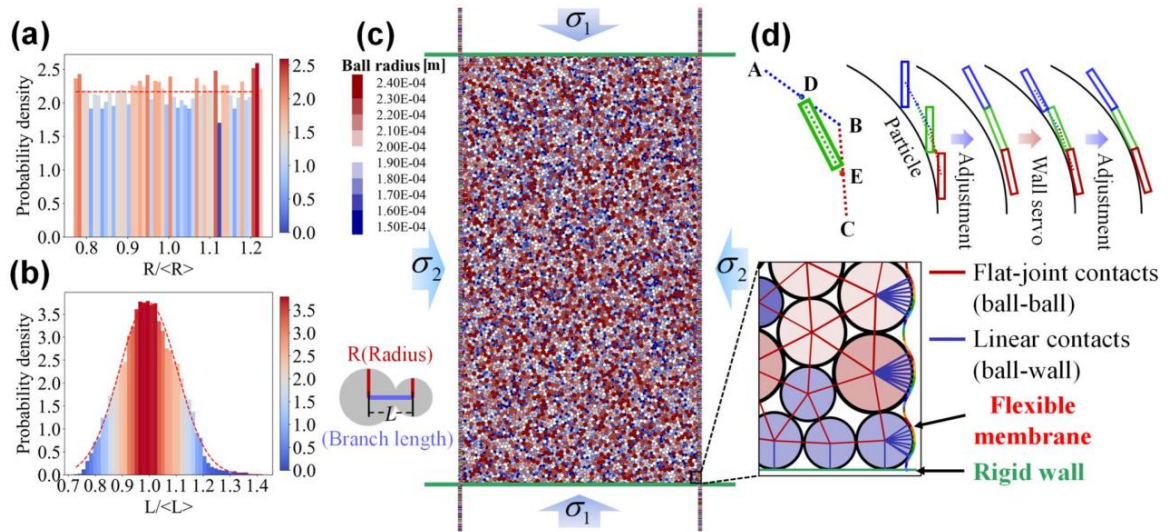


Fig. 2.10: Numerical model set-up: (a) particle size distribution. (b) branch length distribution, (c) loading scheme, (d) scheme for flexible membrane approach (Zhang & Konietzky, 2025)

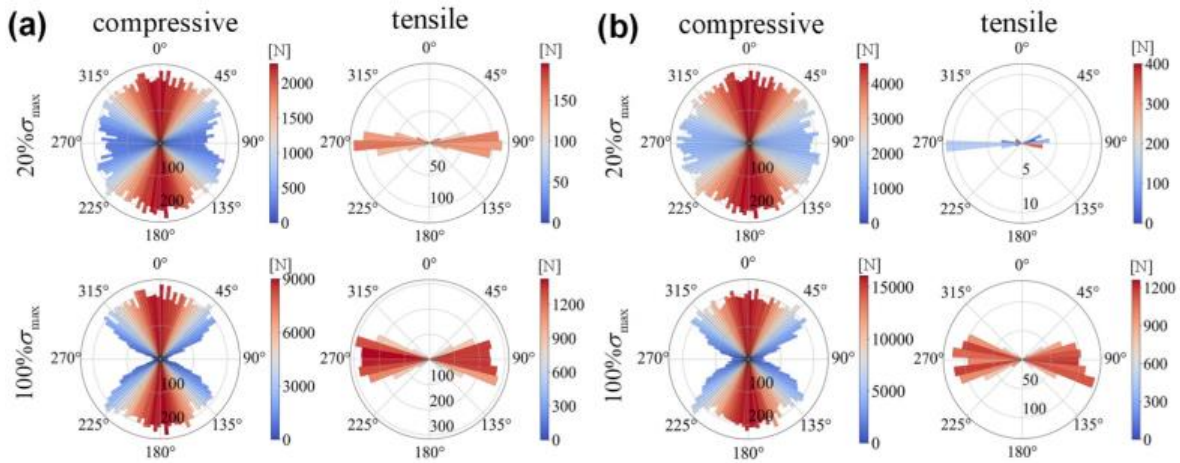


Fig. 2.11: Polar distribution of normal contact forces at different stress states: (a) confining stress of 2.5 MPa and (b) confining stress of 7.5 MPa (Zhang & Konietzky, 2025)

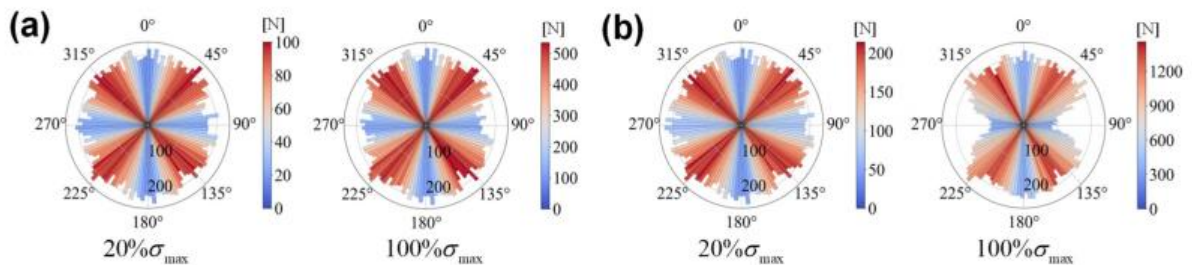


Fig. 2.12: Polar distribution of normal contact forces at different stress states: (a) confining stress of 0 MPa and (b) confining stress of 5 MPa (Zhang & Konietzky, 2025)

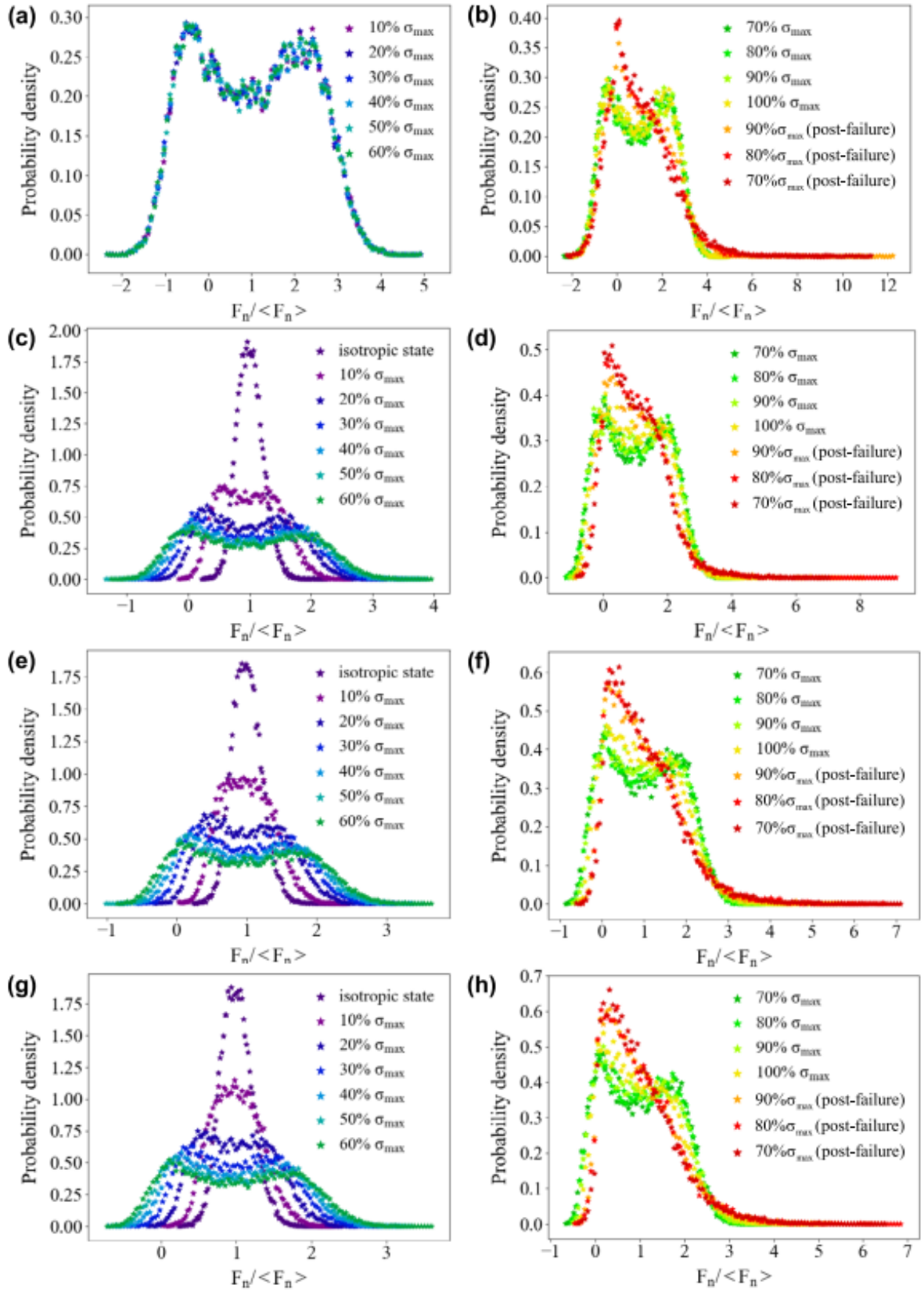


Fig. 2.13: Probability densities of normalized normal contact forces for samples under biaxial loading and different confinement: (a,b) 0 MPa, (c,d) 2.5 MPa, (e,f) 5.0 MPa, (g,h) 7.5 MPa (Zhang & Konietzky, 2025)

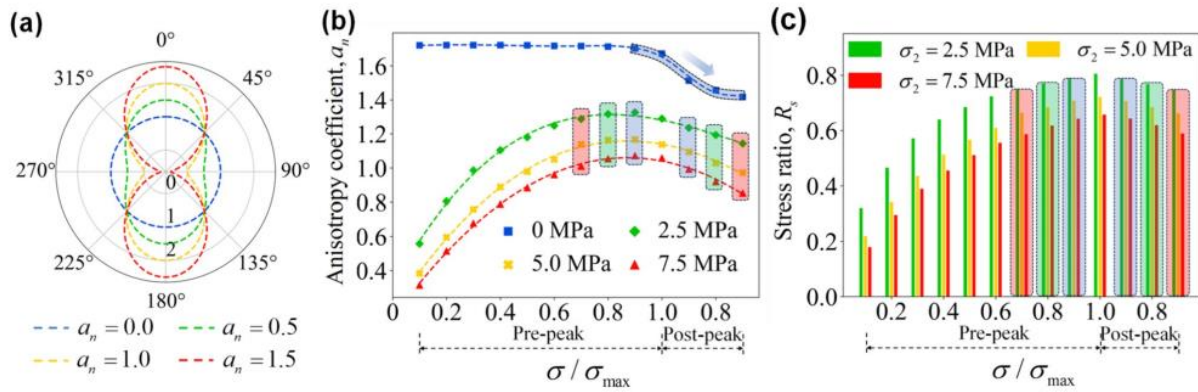


Fig. 2.14: Illustration of evolution of stress (contact force) anisotropy during loading (Zhang & Konietzky, 2025)

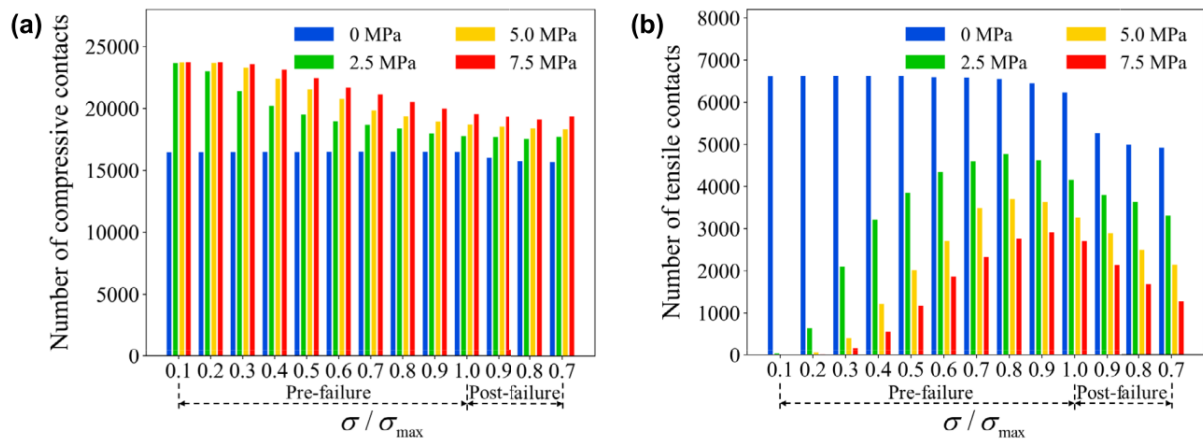


Fig. 2.15: Number of (a) compressive and (b) tensile contacts during loading process (Zhang & Konietzky, 2025)

Further examples are published in papers given in Tab. 2.1.

Tab. 2.1: List of DEM applications with references

Application	References
nuclear test	te Kamp et al. 1998
micromechanics of clay	te Kamp and Konietzky 2002
interlocking geogrids	Konietzky et al. 2004b
microfracturing of metal	Konietzky et al. 2004a
cutting/drilling process	Lunow and Konietzky 2009
granular rock structure	Zhang and Konietzky, 2025
bank protection/bank slope	Herbst et al. 2010
crushing process	Al-Khasawneh and Konietzky 2010
cracking/micromechanics of concrete	Groh et al. 2011
sand/granular materials	Stahl and Konietzky 2011
soil liquefaction/HM coupling	Jakob et al. 2012

### 3 Smoothed Particles

The method of Smoothed Particle Hydrodynamics (SPH) was introduced by Monaghan 1988 for calculations of astrophysical phenomena. SPH was further developed and it is now also possible to simulate fluids with it. The continuum to be examined is approximated by discrete particles. Every SPH particle has a core, that is described by a kernel function  $W(x, h)$  (also called smoothing kernel or interpolating kernel). Here  $h$  is the effective area of a particle and  $x$  is the distance to the centre. The kernel function in one-dimensional case can e.g. be a Gaussian distribution (see 3.1).

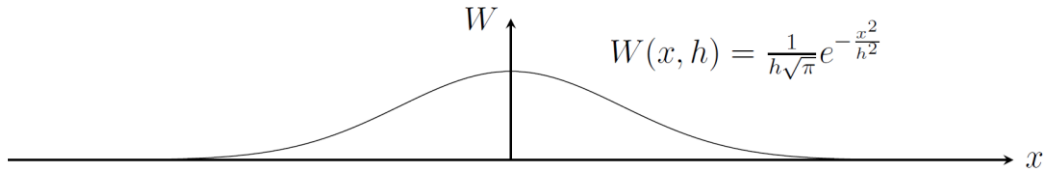


Fig. 3.1: Gauss kernel

The particles are attributed to physical quantities density  $\rho$ , position  $\vec{x}$  and velocity  $\vec{v}$ . These must be recalculated in every time step.

#### 3.1 Interpolation

The integral interpolant of any function  $A(\vec{x})$  is defined as

$$A(\vec{x}) = \int A(\vec{x}') W(\vec{x} - \vec{x}', h) d\vec{x}' \quad (25)$$

whereby it is integrated over the whole space and kernel function  $W$  has following properties (Monaghan 1992).

$$\int W(\vec{x} - \vec{x}', h) d\vec{x}' = 1 \quad \text{and} \quad \lim_{h \rightarrow 0} W(\vec{x} - \vec{x}', h) = \delta(\vec{x} - \vec{x}') \quad (26)$$

The integral interpolant of field variable  $A$  of one SPH particle at position  $\vec{x}$  can be approximated by a summation interpolation of its neighbor particles ( $b$ ).

$$A(\vec{x}) = \sum_b A_b \frac{m_b}{\rho_b} W(\vec{x} - \vec{x}_b, h) \quad (27)$$

$m_b$ ,  $\rho_b$ ,  $A_b$  and  $\vec{x}_b$  are mass, density, value of the field variable and position vector of neighbor particles. The gradient of  $A$  is determined by

$$\nabla A(\vec{x}) = \sum_b A_b \frac{m_b}{\rho_b} \nabla W(\vec{x} - \vec{x}_b, h) \quad (28)$$

Therefore, in SPH method no mesh is needed for calculation of partial derivatives (meshless method).

### 3.2 Physics of SPH-Particles

Required derivatives  $\nabla \cdot \vec{v}$  and  $\nabla p$  for mass conservation (continuity equation)

$$\frac{\partial \rho}{\partial t} + \rho \nabla \cdot \vec{v} = 0 \quad (29)$$

and momentum conservation

$$\frac{\partial \vec{v}}{\partial t} + \frac{1}{\rho} \nabla p = 0 \quad (30)$$

results with  $\vec{v}_{ba} = \vec{v}_b - \vec{v}_a$  and  $W_{ab} = W(\vec{x}_a - \vec{x}_b)$  from summation interpolation (see Eq.(28)). It applies for all particles  $a$

$$(\nabla \cdot \vec{v})_a = \sum_b \frac{m_b}{\rho_b} \vec{v}_{ba} \nabla W_{ab} \quad (31)$$

and

$$(\nabla p)_a = \sum_b \frac{m_b}{\rho_b} \vec{p}_b \nabla W_{ab} \quad (32)$$

in which density is given by

$$\rho(\vec{x}) = \sum_b m_b \nabla W(\vec{x} - \vec{x}_b, h) \quad (33)$$

Consequently, discrete form of continuity equation is given by

$$\frac{\partial \rho_a}{\partial t} = \rho_a \sum_b \frac{m_b}{\rho_b} \vec{v}_{ab} \nabla W_{ab} \quad (34)$$

and discrete form of momentum conservation by

$$\frac{\partial \vec{v}_a}{\partial t} = -\frac{1}{\rho_a} \sum_b \frac{m_b}{\rho_b} \vec{p}_b \nabla W_{ab} \quad (35)$$

The particle velocity  $\vec{v}$  arises from derivative

$$\vec{v}_a = \frac{\partial \vec{x}_a}{\partial t} \quad (36)$$



### 3.3 Examples

SPH comes often into operation in computer animations with water, because with SPH very realistic results can be obtained.



Fig. 3.2: Water simulation with SPH (source: Bell et al. 2005)

Another example shows the so-called “Millennium Simulation”, that simulates the formation of big scale mass distributions in space (galaxies and galaxy clusters). For this calculation more than 10 billion particles were used (see <http://www.mpa-garching.mpg.de/galform/millennium/>).

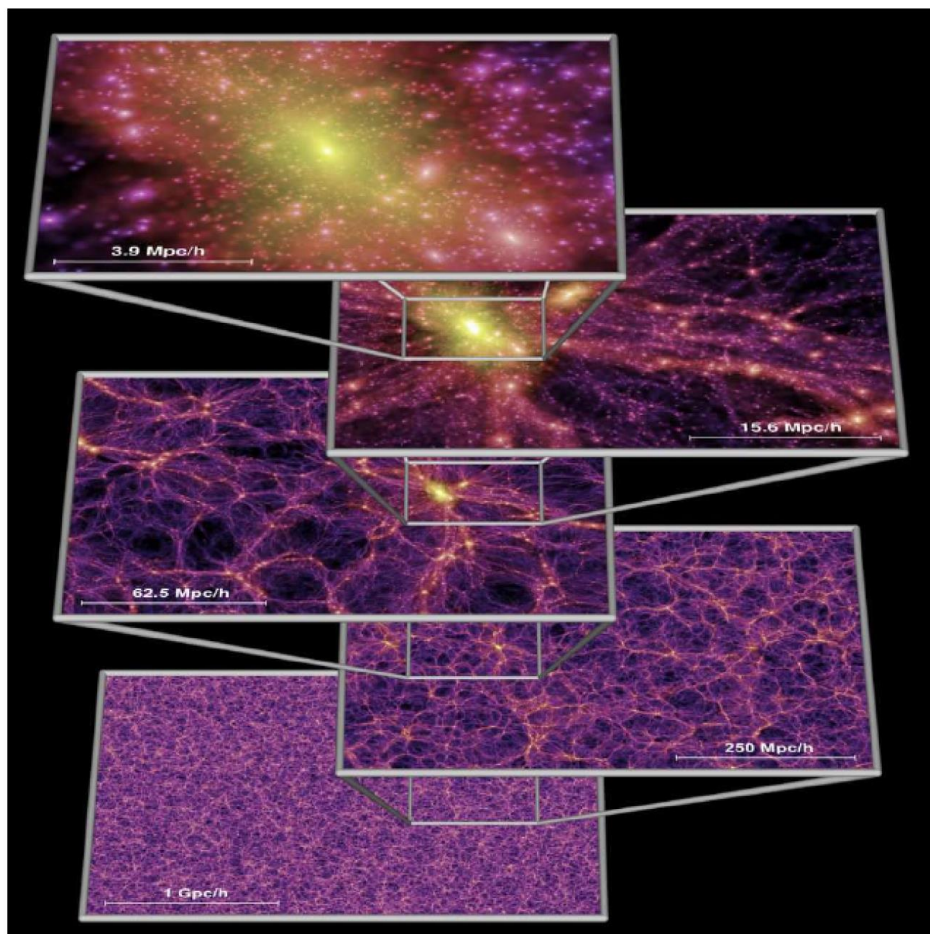


Fig. 3: “Millennium Simulation” with  $> 10^{10}$  particles (source: Springel et al. 2005)



## 4 Lattice Boltzmann

The Lattice Boltzmann Method (LBM) is based on the theory of Ludwig Boltzmann (1844-1906). Boltzmann treats a gas as medium, that consists of interacting particles (molecules or atoms), that can be described with classical mechanics and a statistical treatment. This basic idea was adopted into LBM, where gases are simulated by streaming and collisions of particles (Sukop and Thorne 2006). The approach was later extended on simulation of fluids in general (gases and liquids).

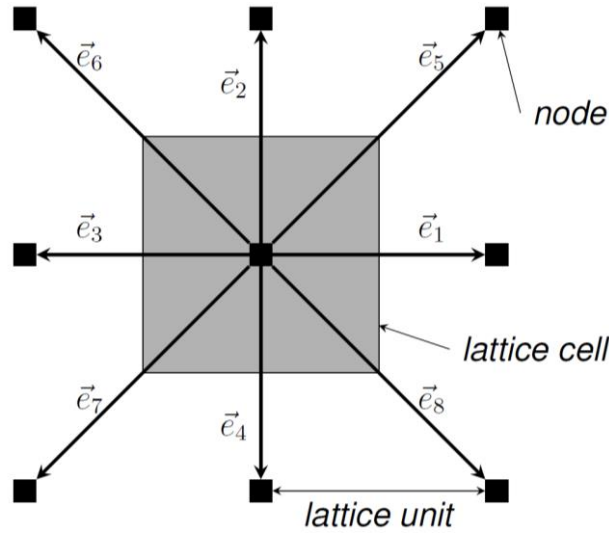


Fig. 4.1: Lattice array for a D2Q9 model

For LBM a lattice consisting of nodes is needed. In 4.1 the lattice array for a D2Q9 model (2 dimensions, 9 nodes) is illustrated. The vectors  $\vec{e}_i$  denotes particle velocities in direction  $i$ . In the simplest approach particles have a uniform mass ( $mu$  - mass unit) and the lattice has uniform lattice spacing ( $lu$  - lattice unit).

### 4.1 Boltzmann equation

A system consisting of  $N$  particles (molecules) can be described by a density function  $F(\vec{x}, \vec{e}, t)$ . When positions  $\vec{x}$  and velocities  $\vec{e}$  of all particles (molecules) are known at time  $t$ , so it is (at least hypothetical) possible to predict the mechanical behavior of the system. Assuming that an external force  $f$  is acting on the particles, then they have positions  $\vec{x} + \vec{e}dt$  and velocities  $\vec{e} + fdt$  at time  $t + dt$ . When no collisions occurred, then it applies

$$F(\vec{x}, \vec{e}, t) d\vec{x} d\vec{e} = F(\vec{x} + \vec{e}dt, \vec{e} + fdt, t + dt) d\vec{x} d\vec{e} \quad (37)$$

If there are collisions within the time step, Eq. (37) is added by a collision term  $\Omega$ , which describes changing rate between end and start condition of the system (Mohamad 2007).

$$F(\vec{x}, \vec{e}, t) d\vec{x} d\vec{e} = F(\vec{x} + \vec{e} dt, \vec{e} + f dt, t + dt) d\vec{x} d\vec{e} + \Omega(F) d\vec{x} d\vec{e} dt \quad (38)$$

The time derivative of Eq. (38) gives

$$\frac{dF}{dt} = \Omega(F) \quad (39)$$

i.e. total changing rate of density function is equal to collision rate. When  $F$  is a function of  $\vec{x}$ ,  $\vec{e}$  and  $t$ , then it applies

$$dF = \frac{\partial F}{\partial \vec{x}} d\vec{x} + \frac{\partial F}{\partial \vec{e}} d\vec{e} + \frac{\partial F}{\partial t} dt \quad (40)$$

Dividing Eq. (40) with  $dt$ , one gets

$$\frac{dF}{dt} = \frac{\partial F}{\partial \vec{x}} \frac{d\vec{x}}{dt} + \frac{\partial F}{\partial \vec{e}} \frac{d\vec{e}}{dt} + \frac{\partial F}{\partial t} \quad (41)$$

With velocity  $\vec{e} = d\vec{x}/dt$ , acceleration  $\vec{a} = d\vec{e}/dt$ , second law of Newton  $\vec{a} = f/m$  (mass  $m$ ) and Eq. (39) it offers Boltzmanns law of motion (Mohamad 2007).

$$\frac{\partial F}{\partial t} + \frac{\partial F}{\partial \vec{x}} \vec{e} + \frac{f}{m} \frac{\partial F}{\partial \vec{e}} = \Omega \quad (42)$$

#### 4.2 Time relaxation according to Bhatnagar, Gross and Krook

The exact calculation of collision term  $\Omega$  in Eq. (42) is very complicated because of its complexity. Therefore  $\Omega$  is approximated by a simple operator, that does not bring significant errors to the solution. Bhatnagar, Gross and Krook (BGK) presented in 1954 a simplified model for the collision operator (Mohamad 2007). Thereby local equilibrium distribution function  $F^{eq}$  and a relaxation factor  $\tau$  were introduced.

$$\Omega = \frac{1}{\tau} (F^{eq} - F) \quad (43)$$

With this approximation (see Eq. (38)) and discretization (index  $i$ ) one gets the linearized BGK relaxation form of LB equation (Cook and Noble 2004).

$$\underbrace{F_i(\vec{x} + \vec{e}_i dt, t + dt)}_{\text{streaming}} = \underbrace{F_i(\vec{x}, t) - \frac{dt}{\tau} (F_i(\vec{x}, t) - F_i^{eq}(\vec{x}, t))}_{\text{collision}} \quad (44)$$

Eq. (44) consists of a streaming and a collision part. At every node there are eight density distributions  $F_i$  and a residual distribution  $F_0$ . Equilibrium conditions are, according to Sukop and Thorne 2006, given by

$$F_i^{\text{eq}}(\vec{x}) = a_i \rho(\vec{x}) \left( 1 + 3 \frac{\vec{e}_i \cdot \vec{v}_f}{c^2} + \frac{9}{2} \frac{(\vec{e}_i \cdot \vec{v}_f)^2}{c^4} - \frac{3}{2} \frac{v_f^2}{c^2} \right) \quad (45)$$

Weightings  $a_i$  are 4/9 for the residual particles with  $i = 0$ , 1/9 for  $i \in \{1, 2, 3, 4\}$  and 1/36 for  $i \in \{5, 6, 7, 8\}$ .  $c$  is basic speed on nodes and macroscopic density  $\rho$  is defined as sum over all directional densities ( $\rho = \sum_i F_i$ ). Macroscopic velocity  $\vec{v}_f$  is the average of microscopic velocities  $\vec{e}_i$  weighted with densities  $F_i$ .

$$\vec{v}_f = \frac{1}{\rho} \sum_{i=0}^8 F_i \vec{e}_i \quad (46)$$

### 4.3 Examples

A LBM application of Schenkengel and Vrettos 2011 simulates an induced soil liquefaction. The 2D model consists of  $300 \times 60$  nodes and represents a slope with a slope angle of  $18^\circ$ . An explosion within the slope leads to stability failure, whereby the material liquefies. Following figure shows velocities of the material at times  $t = 0.01$  s,  $t = 0.29$  s and  $t = 1.17$  s during liquefaction event.

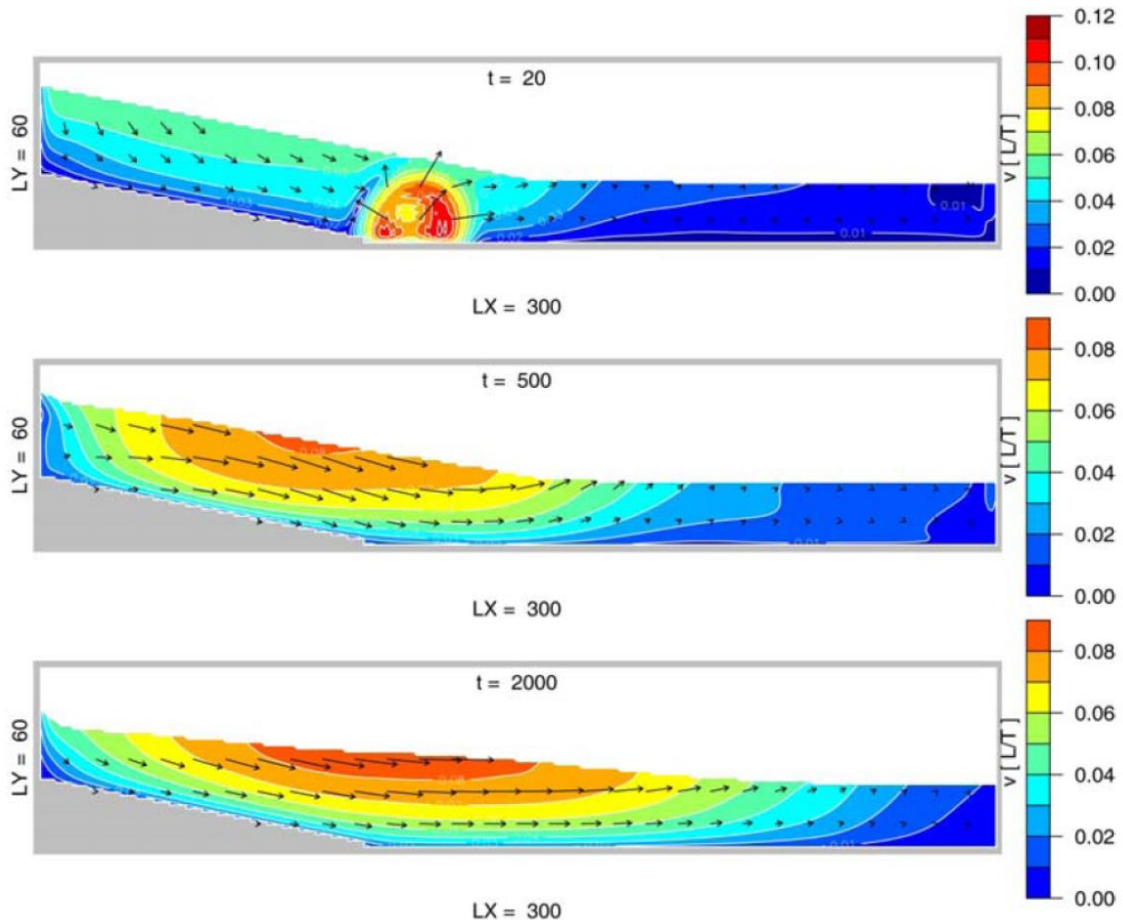


Fig. 4.2: 2D-LBM model of an explosion within a slope, velocities in the lattice illustrated by vectors and filled colored contours (source: Schenkengel and Vrettos 2011)

With the model of Schenkengel and Vrettos 2011 at first time rheological transition from rigid to liquid was solved and implemented in a model with a LBM approach.

Another example shows a phase separation of two fluids with different density.

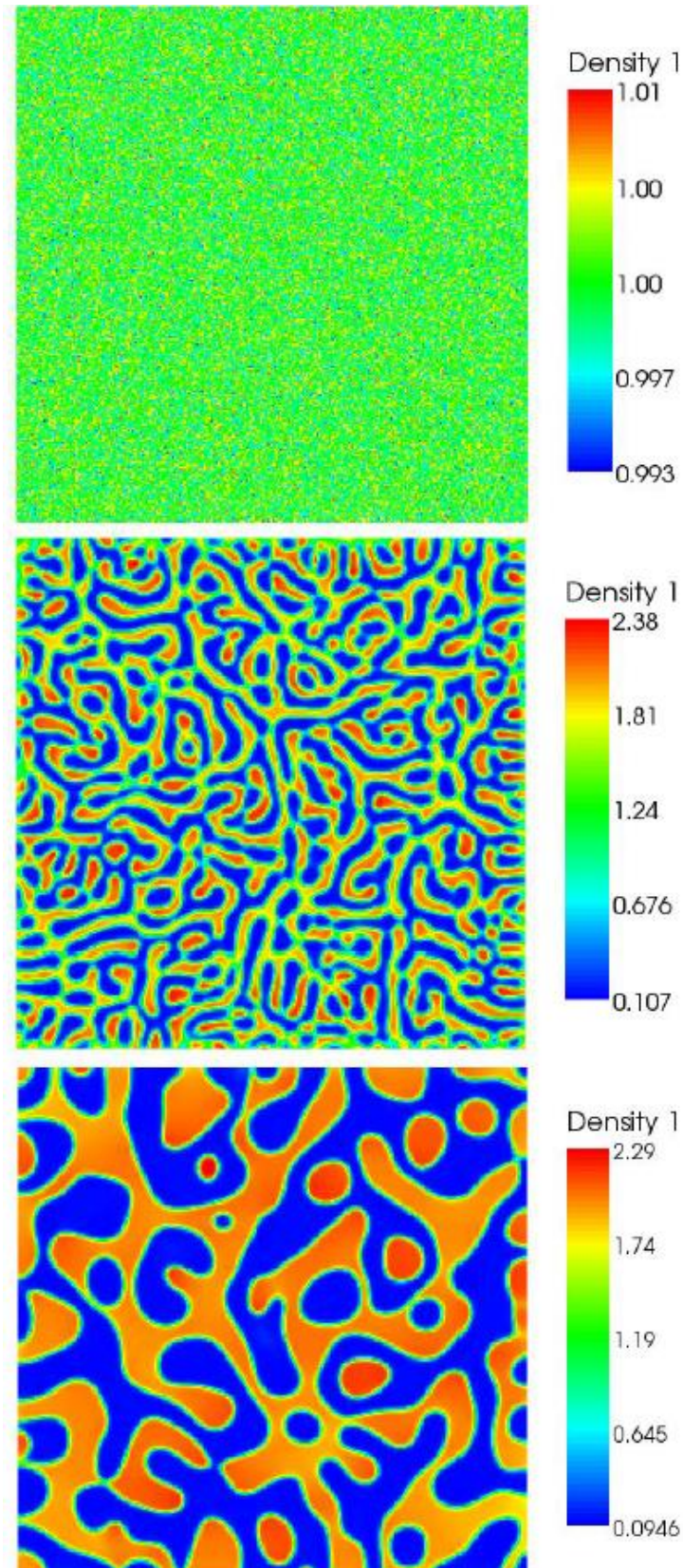


Fig. 4.3: Phase separation of two fluids (source: <http://www.bgce.de/curriculum/projects/patilgmeiner/>)



## 5 Molecular Dynamics

With Molecular Dynamics (MD) interactions between atomic particles (atoms, molecules, nanoparticles, etc.) can be simulated. The laws of classical mechanics find no more validity. For description of particle mechanics, laws of quantum mechanics must be used. Anyhow DEM and MD are very similar.

The first application of MD is dated to the year 1957 with a paper by Alder and Wainwright. Hence MD is the oldest applied particle method. Compared to DEM, where Newton's equations serves as basic principle of description of particle motion, MD is based on Schrödinger equation. It is a very complex equation and can be solved analytically only in rarest cases. Even numerical approaches limit applications of the Schrödinger equation to very simple systems and few particles. So approximation procedures are used to simplify solving of the equation (Griebel et al. 2004).

### 5.1 Schrödinger equation

In quantum-mechanical systems conclusions about the state of the system can be derived by a state function  $\Psi$  (also called wave function). A system consisting of  $N$  cores and  $K$  electrons with variables  $R_i$  resp.  $r_i$  is characterized by its state function as follows (Griebel et al. 2004).

$$\Psi = \Psi(R_1, \dots, R_N, r_1, \dots, r_K, t) \quad (47)$$

Variable  $t$  indicates time dependency of the state function.  $\Psi$  is due to solution of the Schrödinger equation (with  $R = R_1, \dots, R_N$  and  $r = r_1, \dots, r_K$ ).

$$i\hbar \frac{\partial \Psi(R, r, t)}{\partial t} = \hat{H} \Psi(R, r, t) \quad (48)$$

Here,  $i$  is imaginary unit,  $\hat{H}$  is the Hamilton operator and  $\hbar = h/2\pi$  with  $h$ , the Planck's constant. The Hamilton operator describes temporal evolution of possible energy values in the system based on its potentials.

### 5.2 Potentials

Interactions between two particles, that depend only on particle distance, are described by pair-potentials. Such potentials are e.g. the gravity potential, the Coulomb potential (electrical point charge), the van-der-Waals potential (weak attraction at inert gases) and the Lennard-Jones potential (uncharged, unbound atoms).

The Lennard-Jones potential

$$U(r_{ij}) = \alpha \varepsilon \left[ \left( \frac{\sigma}{r_{ij}} \right)^n - \left( \frac{\sigma}{r_{ij}} \right)^m \right], m < n \quad (49)$$

With  $\alpha = \frac{1}{n-m} \left( \frac{n^n}{m^m} \right)^{\frac{1}{n-m}}$  is parameterized by  $\sigma$  and  $\varepsilon$ . Here  $\varepsilon$  defines the magnitude of repulsion resp. attraction forces. Thus, materials of different stiffnesses can be simulated.  $\sigma$  specifies zero-crossing of the potential. 5.1 shows a Lennard-Jones potential for  $n = 12$  and  $m = 6$ .

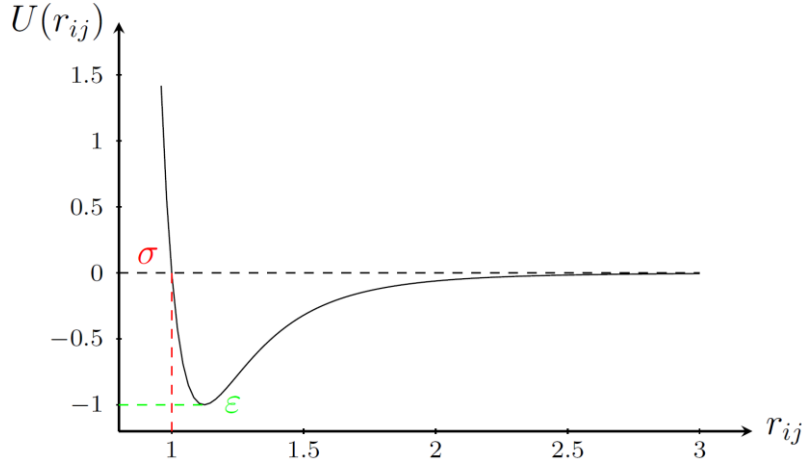


Fig. 5.1: Lennard-Jones potential with  $\varepsilon = 1$  and  $\sigma = 1$

If a particle moves within a potential, the corresponding potential energy is due to

$$E_{\text{pot}}(R) = \sum_{i=1}^N \sum_{j=1, j>i}^N U_{ij}(r_{ij}) \quad (50)$$

where  $r_{ij} = \|R_j - R_i\|$  is the distance between particles. The potential function for the Lennard-Jones potential with  $n = 12$  and  $m = 6$  is

$$E_{\text{pot}}(R) = 4 \cdot \varepsilon \sum_{i=1}^N \sum_{j=1, j>i}^N \left[ \left( \frac{\sigma}{r_{ij}} \right)^{12} - \left( \frac{\sigma}{r_{ij}} \right)^6 \right] \quad (51)$$

The corresponding force  $\vec{F}_i$ , which acts on particle  $i$ , results by creation of a gradient with respect to  $R_i$ .

$$\vec{F}_i = -\nabla_{R_i} E_{\text{pot}}(R) \quad (52)$$

For the Lennard-Jones potential this force is given by the equation

$$\vec{F}_i = 24 \cdot \varepsilon \sum_{j=1, j \neq i}^N \frac{1}{r_{ij}^2} \cdot \left( \frac{\sigma}{r_{ij}} \right)^6 \cdot \left( 1 - 2 \cdot \left( \frac{\sigma}{r_{ij}} \right)^6 \right) \vec{r}_{ij} \quad (53)$$

where  $\vec{r}_{ij}$  is the directional vector between particles  $i$  and  $j$  (Griebel et al. 2004).

### 5.3 Physics of MD-Particles

Physics of MD-Particles is in general the same as for DEM-Particles (see section 2.3). With Newton's second law accelerations, velocities and displacements are determined by time integration. In doing so one gets new positions of the particles. Unlike in DEM simulations MD-Particles have a cutting radius, which results from potential range. As simplification no forces act on a particle, as long no further particles stay in its potential range.

### 5.4 Examples

In Fig. 5.2 collision of two bodies is displayed. Particle velocities are coded with colors (red - high velocity, blue - low velocity).

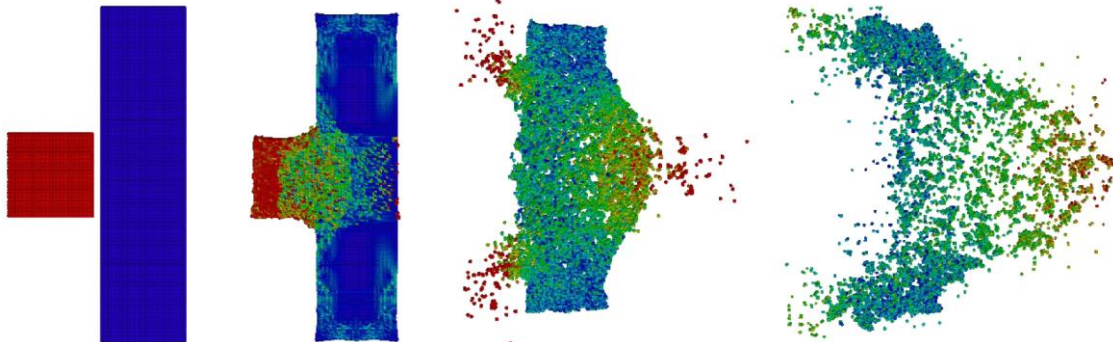


Fig. 5.2: Collision of two bodies, temporal evolution of particle distribution (source: <http://wissrech.ins.uni-bonn.de>)

Lipid molecules typically form double layer membranes in the presence of water, because one end is hydrophilic and the other end is hydrophobic (e.g. oil film). These membranes spontaneously form bubbles or vesicles. Fig. 5.3 shows a simulation of a fusion of such a vesicle with a lipid membrane.

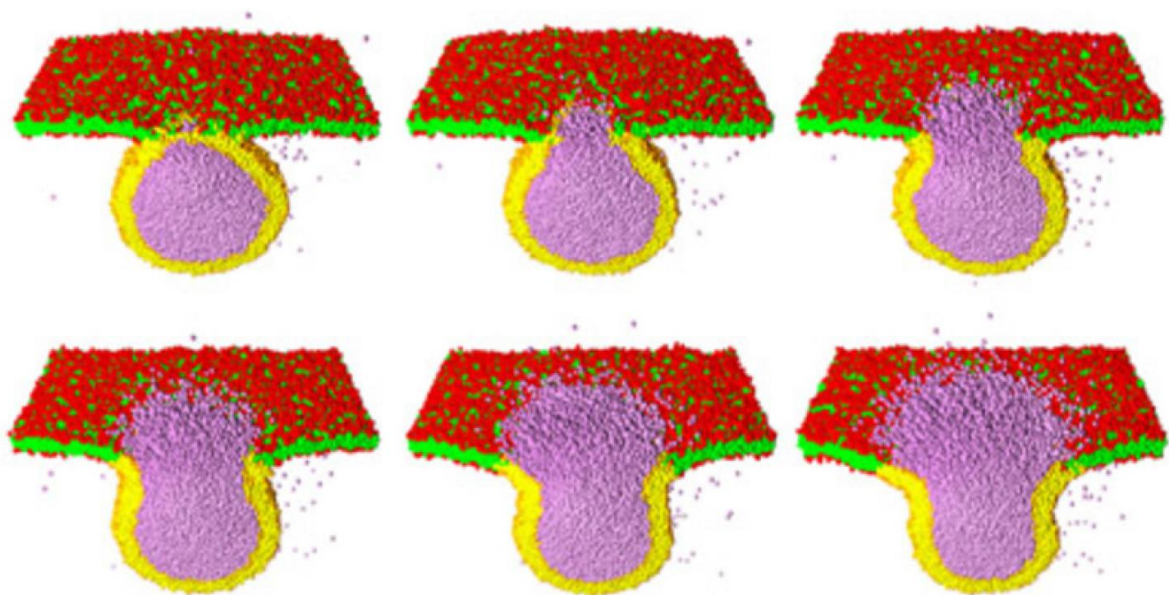


Fig. 5.3: Fusion of one vesicle with a membrane of 2018 Diblock-Copolymers, vesicle diameter 40 nm (source: <http://www.mpg.de>)

## References

- Al-Khasawneh, Y. & Konietzky, H. (2010). "Interpretation and optimization of vertical shaft crushers with DEEM". In: Proceedings European Conference on Fracture (ECF-18), Bundesanstalt für Materialprüfung und -forschung (BAM), Berlin, pp. 1–8.
- Alder, B. & Wainwright, T. (1957). "Phase transition for a hard sphere system". In: Journal for Chemical Physics 27, pp. 1208–1209.
- Bell, N. et al. (2005). "Particle based simulation of granular materials". In: Proceedings of the 2005 ACM SIGGRAPH/Eurographics Symposium on Computer animation.
- Cook, B.K. & Noble, D.R. (2004). "A direct simulation method for particlefluid systems". In: Engineering Computations 21, pp. 151–168.
- Griebel, M. et al. (2004). Numerische Simulation in der Moleküldynamik. Springer. ISBN: 3-540-41856-3.
- Groh, U. et al. (2011). "Damage simulation of brittle heterogeneous materials at the grain size level". In: Theoretical and Applied Fracture Mechanics 55.1, pp. 31–38.
- Herbst, M. et al. (2010). "Numerische Simulation der Interaktion Wasser - Deckwerk im Tidegebiet". In: Wasserbauliche Mitteilungen 40, pp. 85–94.
- Itasca (2008). PFC3D Version 4.0 Theory and Background. Manual.
- Jakob, C. et al. (2012). "Mikromechanische Modellierung verflüssigungsempfindlicher Sande". In: Tagungsband Freiburger Forschungsforum - FK 4: Bodenverflüssigung bei Kippen des Lausitzer Braunkohlebergbaus.
- Konietzky, H. et al. (2004a). "Simulation of timedependend damage and microfracturing via particle methods". In: Proceedings ICLODC 2004. SFB 398 Ruhr-University Bochum, pp. 131–140.
- Konietzky, H. et al. (2004b). "Use of DEM to model the interlocking effect of geogrids under static and cyclic loading". In: Numerical Modeling in Micromechanics via Particle Methods. A.A. Balkema Publishers, pp. 3–11.
- Lunow, C. & Konietzky, H. (2009). "Two dimensional simulation of the pressing and the cutting rock destruction". In: Proceedings 2nd Int. Conf. on Computational Methods in Tunneling. Aedificatio Publishers, pp. 223–230.
- Mohamad, A.A. (2007). Applied Lattice Boltzmann Method. Dept. of Mechanical and Manufacturing Engineering, Schulich School of Engineering, The University of Calgary. ISBN: 978-0-9783253-0-5.
- Monaghan, J.J. (1988). "An introduction to SPH". In: Computer Physics Communications 48, pp. 89–96.
- (1992). "Smoothed Particle Hydrodynamics". In: Annual Review of Astronomy and Astrophysics 30, pp. 543–574.
- Schenkengel, K.U. & Vrettos, C. (2011). "Modelling of liquefaction-induced lateral spreading using the Lattice Boltzmann Method". In: 5th International Conference on Earthquake Geotechnical Engineering.
- Springel, V. et al. (2005). "Simulating the joint evolution of quasars, galaxies and thier large-scale distribution". In: Nature 435, pp. 629–636.
- Stahl, M. & Konietzky, H. (2011). "Discrete element simulation of ballast and gravel under special consideration of grain-shape, grain size and relative density". In: Granular Matter 13.4, pp. 417–428.
- Sukop, M.C. & Thorne, D.T. (2006). Lattice Boltzmann Modeling. Springer. ISBN: 3-540-27981-4.



- te Kamp, L. & Konietzky, H. (2002). "Conceptual Micromechanical simulation of stiff clay using particle methods". In: Proceedings 5th European Conference on Numerical Methods in Geotechnical Engineering. LCPC-Press, pp. 315–320.
- te Kamp, L. et al. (1998). "Modeling of the Chagan underground nuclear test with the distinct element method". In: FRAGBLAST 2, pp. 295– 312.
- Zhang, M. & Konietzky, H. (2025): Evolution of force network, contact network, and tensile forces in rock-like bonded granular materials under unconfined and confined compression: A DEM study, *Environmental Earth Sciences*, 84:320